THE JOURNAL OF Ammonia Energy

Available online at

jae.cardiffuniversitypress.org

ISSN **2752-7735**
The Journal of Ammonia Energy 01 (2023) 091–105

Cardiff University Press | Gwasg Prifysgol Caerdydd

Experimental Investigation of Spark-Assisted Compression-Ignition with Ammonia-Hydrogen Blends

Reggeti SA, Kane SP, Northrop WF*

University of Minnesota, Department of Mechanical Engineering, Minneapolis, Minnesota, United States

Abstract

Carbon-free emissions and stable operation of ammonia-fueled internal combustion engines have been demonstrated in recent studies through combustion strategies suited to the fuel's unique properties. High ignition energy and slow flame speed of ammonia are typically compensated for by hydrogen addition and/or enhanced ignition systems while the high octane rating of ammonia allows high compression ratio. The experimental study in this work investigates the performance of ammonia in spark-assisted compression-ignition (SACI) mode, where the cylinder charge is spark ignited and a subsequent auto-ignition event results in a faster burn and more ideal combustion phasing. The high-compression ratio engine was fueled by 100% anhydrous ammonia or blends with small quantities of hydrogen (2.5% and 5% by volume). Fuels were port-injected for a homogeneous intake charge mixture at stoichiometric equivalence ratio. Two different engine speeds were tested at several intake temperatures and spark timings. All cases showed an inflection point in the apparent heat release rate (AHRR) followed by more rapid rate of heat release, signaling the onset of auto-ignition. Blending hydrogen in the fuel benefited gross indicated mean effective pressure (gIMEP) at maximum brake torque (MBT) timing, but pure ammonia fuel was more stable across a wide range of spark timings and intake temperatures. Burn durations in the present study were similar to those of conventional SI engines fueled by gasoline indicating that the combustion enhancement of SACI compensated for the lower flame speed of ammonia. The control of SI percent, defined as the fraction of heat release before auto-ignition compared to the total heat release, is shown to be strongly related to the sensitivity of auto-ignition timing to spark timing. Unburned ammonia emissions are hypothesized to be primarily driven by unburned gases trapped in the crevices and are mitigated slightly through blending hydrogen in the fuel or by increasing intake temperature. However, the addition of hydrogen and increasing intake temperature led to increased nitric oxide (NO) emissions. Of primary concern because of its potent global warming potential, nitrous oxide (N_2O) did not show a clear trend with fuel hydrogen content or intake temperature, but definitively increased for the higher engine speed.

Received: 7th April 23; Accepted: 12th June 23; Published: 4th July 23

Keywords: Ammonia, Spark-Assisted Compression Ignition, Carbon-Free Fuels, Renewable Fuels, Emissions

Introduction

Achieving net-zero carbon emissions to offset the anthropogenic contribution to climate change is a pressing issue in today's society. Numerous major global economies have prioritized carbon neutrality goals including the United States and the European Union pledging to be carbon neutral by 2050 and China by 2060 [1-3]. The paths to achieve these long-term goals are challenging, requiring significant investment in infrastructure and innovation of new technologies. Increasing the share of renewable energy (e.g. wind and solar) is at the heart of these efforts, but energy storage solutions to accommodate fluctuating grid demands and to propel transportation vehicles are vitally important [1]. Among potential carbon-free energy storage solutions, anhydrous ammonia (NH_3) has been gaining popularity recently as it presents distinct storage, energy density, and infrastructure readiness advantages over alternatives such as hydrogen (H_2) and rechargeable batteries.

Today, the scalable, single-step Haber-Bosch Process produces ammonia economically at large scale. Conventionally, methane steam reforming produces hydrogen which is combined with nitrogen obtained by air separation to produce so called, "brown ammonia." Alternatively, hydrogen from water electrolyzers fed by renewable energy can be used to generate completely renewable, "green ammonia" [4]. Ammonia is also already widely distributed worldwide through a well-established infrastructure of pipelines and transportation by ship and by rail [5].

Ammonia can be stored in liquid form by refrigeration to remain below its atmospheric boiling point (240 K) or by pressurized tanks to keep it below its vapor pressure (8.6 bar). Liquid-phase ammonia is energy dense per unit volume (11.3 MJ/L) [4] compared to gaseous hydrogen stored at

* Corresponding author. Tel.: +1-612-625-6854. E-mail address: wnorthro@umn.edu
https://doi.org/10.18573/jae.21

700 bar (4.7 MJ/L) [6] and modern lithium-ion batteries (1.9 MJ/L) [7]. Indeed, hydrogen and rechargeable batteries are crucial to achieve carbon neutrality; however, favorable storage properties of ammonia make it an attractive option for applications in central power, marine propulsion, and agriculture. Recent work has shown that ammonia is knock-resistant and burns favorably in internal combustion engines (ICEs) with high compression ratio (CR) [8,9]. The objective of this work is to investigate combustion and emissions of ammonia in high-CR ICEs for such applications.

Burning ammonia in ICEs goes back nearly a century when ammonia was used to fuel buses during fossil fuel shortages in World War II. While developed out of necessity, the fleet of buses fueled by ammonia and coal gas (a combustion promoter) performed similarly to the gas-oil engines of the time with no appreciable loss in power or excessive wear on the engines [10]. Additional investigations in the 1960s explored ammonia use in both spark ignition (SI) and compression ignition (CI) engines (e.g. [11,12]). These studies showed optimal engine performance with a SI platform which benefited from a high-ignition energy spark plug, high compression ratio, supercharging, and/or hydrogen addition as a combustion promoter.

In recent years, renewed interest in ammonia utilization through combustion has produced an array of scientific studies with modern ICE and emission control strategies. Grannell *et al.* investigated combustion stability by partially replacing gasoline with ammonia in a SI engine operating at CRs from 8:1 to 12:1. Up to 70% of fuel energy could be supplied by NH_3 at wide open throttle and the knock-resistance of NH_3 yielded greater IMEP and efficiency at high load, yet 100% gasoline was needed for stable running at idle [13]. High energy replacement of gasoline with a direct-injected ammonia system was demonstrated by Ryu *et al.*, but pollutant emissions increased compared to pure gasoline operation [14]. Gill *et al*. employed a CI engine platform with NH_3 fumigation in the intake air which resulted in decreased diesel consumption and CO emissions, but increased N_2O – a greenhouse gas 300 times as potent as CO_2 [15]. Kane *et al.* showed an increased energy replacement of diesel fuel with fumigated NH_3 by recovering exhaust waste heat to drive an ammonia decomposition catalyst, partially converting NH_3 to H_2. CO_2 emissions were reduced and brake thermal efficiency (BTE) was improved for low engine speeds while soot, unburned hydrocarbons, NO_x and NH_3 emissions generally increased with increasing fumigant energy fraction [16].

Rather than blending with conventional fossil fuels, other researchers have blended ammonia with hydrogen, a carbon free fuel with better combustion promoting characteristics (i.e. wide flammability limits, high laminar flame speed, low ignition energy). Lhuillier *et al.* investigated SI engine operation (10.5:1 CR) NH_3/H_2 blends ranging from 0-60% H_2 by volume. Results showed that the best IMEP was achieved with a 20% H_2 fraction since increasing H_2 further led to excessive heat loss [17]. Since onboard hydrogen storage could be impractical on a vehicle due to high cost and low energy density, several works have focused on identifying the minimum H_2 fraction for stable engine operation. Frigo *et al.* investigated the stable operating limits of a twin-cylinder engine operating at 10.7:1 CR, fueled by NH_3/H_2 blends. The minimum H_2 to NH_3 energy fraction was about 7% at full load and 11% at half load (9.5% and 15% by volume, respectively) [18]. Mounaïm-Rousselle *et al.* also demonstrated the load-dependence of fuel H_2 fraction in a modern gasoline direct injected (GDI) SI engine (10.5:1 CR) and noted that at least 10% H_2 by volume was needed at low load, and that 100% ammonia operation was not possible at engine speeds in excess of 2000 rpm [19]. Overall, recent literature suggests that H_2 addition of nominally 10% by volume is needed as a combustion promoter for conventional SI engine architecture, but engine load and speed greatly impact H_2 requirements.

Hydrogen for blending with ammonia fuel could be provided by an onboard ammonia reforming system. Ammonia decomposition to H_2 is an endothermic process which requires external heating and a catalyst for the reactions to proceed at the necessary rates for an ICE. Comotti *et al.* utilized a commercial ruthenium catalyst which was heated by high temperature exhaust gases and by electrical heaters to maintain catalyst temperatures above 673 K [20]. Kane *et al.* housed the ammonia decomposition catalyst in a diesel oxidation catalyst to leverage both the sensible heat in the exhaust gases and the heat produced by the oxidation of unburned ammonia and diesel fuel in the exhaust [16]. Alternatively, exothermic partial oxidation of ammonia upstream of the engine provides necessary heat for the endothermic hydrogen production reactions [21]. While effective, especially when paired with a catalyst, the partial oxidation approach consumes additional fuel to provide heat. In recent work, Reggeti *et al.* demonstrated that in-cylinder reforming of ammonia at fuel-rich equivalence ratios could produce H_2 fractions in the exhaust of ~8% while generating useful work [9]. Hydrogen-rich exhaust gases could be recirculated to the intake through a dedicated exhaust gas recirculation (dEGR) strategy, as described by [22].

Considering the challenges of managing and generating a significant amount of H_2 for an ICE,

ammonia has been tested in high-compression ratio engines to mitigate the H_2 required for stable operation. Mounaïm-Rousselle *et al.* leveraged the high CR of a diesel engine and adapted it for SI operation by putting a spark plug in the engine head. Compression ratios from 14:1 to 17:1 enabled stable operation with intake-fumigated 100% ammonia which was compared to a SI case with 10% H_2 by volume in a 10:1 CR engine. The high CR in this study achieved similar combustion phasing to the hydrogen-enriched, low-CR case and showed improved COV for low loads and high engine speeds. Mounaïm-Rousselle et al. suggest that the enhanced combustion processes with high compression ratio resulted because the engine was operating in a mode known as spark-spark assisted compression-ignition (SACI) [8].

A combination of conventional SI and homogeneous charge compression ignition (HCCI), SACI utilizes a spark to initiate combustion which helps trigger auto-ignition in the unburned gas mixture. The spark induces a deflagration flame front providing the energy for auto-ignition which quickly consumes the remaining charge [23]. SACI mode has a characteristic dual-mode heat release from slow burning deflagration, followed by a more intense auto-ignition heat release. Conventional SI engines rely on propagation of the deflagration flame front throughout the whole combustion chamber to release heat, but the slow flame speed of ammonia makes this unfeasible without a combustion promoter (e.g. H_2). Besides serving to speed up the combustion process, SACI has been shown to improve efficiency by the combination of high dilution, increased ratio of specific heats, reduced pumping losses, and knock mitigation, enabling higher compression ratios [24]. The high knock resistance of ammonia lends itself to operate favorably in this combustion mode with little or no hydrogen blending. The objective of this study is to evaluate ammonia combustion in SACI mode for a wide range of operation parameters.

The following section details the experimental apparatus and the methods for experimentation and analysis. Next, the results of the study are presented including analysis of the combustion process and emissions. Finally, findings are summarized and conclusions are drawn from the present work in the last section.

Materials and Methods

A Waukesha Cooperative Fuel Research (CFR) octane engine that features an adjustable CR is the platform for experiments in this study. The cylinder head can be moved relative to the engine block to change the clearance volume, varying CR from a minimum of 4:1 to a maximum of 18:1. A fixed CR of 18:1 was selected for the present study. Figure 1 shows the CFR engine combustion chamber layout. The engine head houses the two valves and the flat-top piston minimizes turbulence and its effect on fuel knock. The spark plug is side-mounted and spark access to the combustion chamber is partially occluded by the piston when at top dead center. Opposite the spark plug, a top-mounted, high-speed pressure transducer (Kistler 6125B) provides in-cylinder pressure data sampled every 0.1 crank-angle degrees (CAD).

The schematic in Fig. 2 shows the air and fuel flow control apparatus, engine control, and data acquisition systems. Clean, dry air was supplied to the engine through a centralized compressed air system, which was purified using pressure-swing absorption to remove moisture and carbon dioxide. Air flow was controlled using a Brooks 5853E mass flow controller (MFC), and flow pulsations were dampened using a 30-gallon steel tank as a plenum resonator. Intake air was heated using an Omega AHPF-101 process heater then mixed with room temperature NH_3 and H_2 (metered by MFCs) before entering the engine. Intake temperature was held steady using a PID controller, with a thermocouple positioned directly at the heater outlet. Temperature and pressure were measured again directly upstream of the intake valve to measure any charge cooling from mixing with fuel(s) or ambient losses. All temperature measurements were performed using Omega Type-K thermocouples, and low-speed pressure measurements were taken using Omega PX419 pressure transducers.

NH_3 and H_2 fuels were metered at steady conditions using a Brooks 5851 MFC and an Alicat Scientific MC-20SLPM-D MFC, respectively. Fuel-air stoichiometry was controlled by proportionately setting air, NH_3, and H_2 flow rates under steady engine conditions. Intake flows and ignition controls, including low speed pressure/temperature data acquisition, were managed using a cRIO-9074 coupled to LabVIEW. Simultaneously, a National Instruments PXI-1042 coupled to a separate LabVIEW program was used as the high-speed data acquisition system for in-cylinder pressure and intake manifold pressure data.

Exhaust NH_3, water, oxygen, and oxides of nitrogen (NO_x and N_2O) were measured using an AVL i60 SESAM FT emissions bench consisting of a Fourier transform infrared spectrometer (FTIR), and a paramagnetic oxygen detector (PMD). High concentrations of NH_3 in the exhaust interfered with accurate measurement of other species using FTIR, so exhaust was diluted using clean dry air from the centralized system. Dilution was accomplished using an Air-Vac TD260h vacuum ejector and orifice plate.

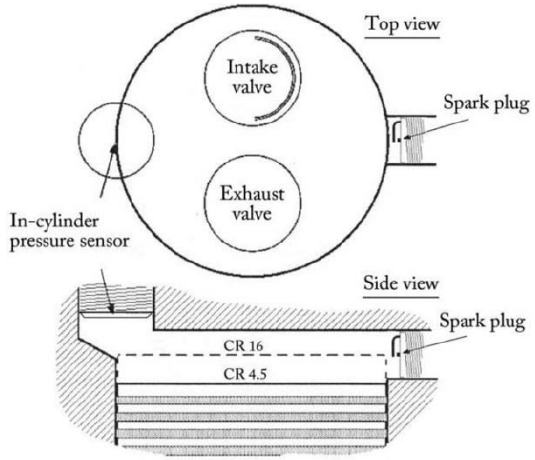

Fig. 1. Valves and access ports of the CFR engine. The top schematic shows an above view of the cylinder head. The bottom schematic shows a side view of the combustion chamber where the piston is shown at the bottom of the schematic, and a dashed line shows the piston position at TDC for a higher CR.

The PMD was insensitive to NH_3 concentration, thus measurement of diluted and undiluted exhaust O_2 was used to determine excess oxygen in the exhaust as well as to calculate dilution ratio (DR) of the FTIR measurement. This calculation for generic species "n" is described in Eqs. (1) and (2) [9]. Undiluted exhaust O_2 was measured for each test, but FTIR measurements (NH_3, NO_x, etc.) were sampled in dilution mode only for maximum brake torque (MBT) timings for each operating condition.

$$DR = \frac{X_{O_2,dilute} - X_{O_2,non-dilute}}{X_{O_2,air} - X_{O_2,dilute}} \quad (1)$$

$$X_n = (DR + 1) * X_{n,dilute} \quad (2)$$

Exhaust sample dilution is the dominant source of uncertainty for emissions measurements with the FTIR, thus precision and bias uncertainties of the dilute samples are neglected in uncertainty analysis. The uncertainty of each emission (δX_n) is determined by Eq. (3) [9],

$$\delta X_n = \frac{\partial X_n}{\partial DR} \delta DR \quad (3)$$

where, δDR is the uncertainty in dilution ratio, calculated by combining the precision uncertainties of $X_{O_2,air}$ (taken over 10 minutes of sampling), $X_{O_2,non-dilute}$, and $X_{O_2,dilute}$ (each over one minute of sampling).

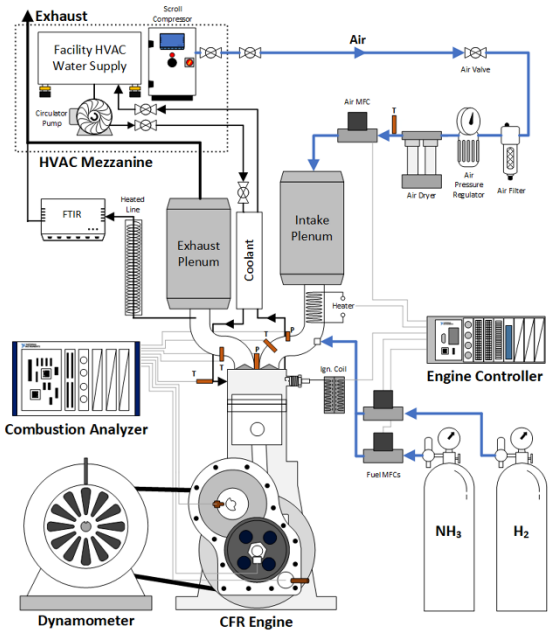

Fig. 2. Layout of components for CFR engine experiments. Dry compressed air and fuel (NH_3 gas and H_2) are metered by MFCs, and intake temperature is controlled by an in-line electrical heater before the intake manifold. The exhaust is sampled by the AVL emissions bench. High speed pressure and encoder data are measured with 0.1 CAD resolution.

Ambient temperature and pressure surrounding the engine were held constant during testing by test-cell air handling. The engine was warmed up to steady-state operating temperatures by firing the engine and accelerated by an electrical heating circuit in the engine oil before collecting data. Stable operating temperatures and test conditions are summarized in Table 1. CR was held constant for all experiments at 18:1 to promote SACI mode at all conditions and to investigate the effects of fuel, intake temperature and spark timing on the SACI combustion mode. Fuel blends were nominally 0%, 2.5%, and 5% H_2 fraction by volume, with equivalence ratio and cylinder trapped mass held constant for all test conditions. Since air and fuel flows were metered with MFCs, intake pressure was allowed to vary when testing different intake temperatures to compensate for changes in intake mixture density. Average intake pressures increased from about 1.07 bar with 40°C intake temperature, to about 1.17 bar with 100°C intake temperature to maintain the same mass flow rate.

For each fueling and temperature condition, spark timing swept from MBT-3 CAD (retarded timing) through MBT+3 CAD (advanced timing) for seven total experiments, unless advancing all the way to MBT+3 resulted in excessive ringing intensity. Pressure traces over 300 cycles were taken at each

test point as well as O_2 emissions measurements. The full suite of FTIR emissions measurements were collected only for MBT timing using the dilution scheme outlined previously.

Table 1. Engine operating conditions and (±) standard deviations when available.

Parameter	Value	Units
Engine Speed	900; 1200	[RPM]
Compression Ratio	18:1	[-]
Coolant Temp.	99.8 ± 0.5	[°C]
Engine Oil Temp.	58.8 ± 0.7	[°C]
Fuel Composition	$(1\text{-}X_{H2})*NH_3 + (X_{H2})*H_2$	[-]
H_2 Fuel Fractions (X_{H2})	0	[%]
	2.80 ± 0.04	[%]
	5.03 ± 0.03	[%]
Mass Flow Rate	2.750 ± 0.003	[g/s]
Equivalence Ratio(Φ)	1 (stoichiometric)	[-]
Intake Temp.	40; 60; 80; 100 (± 0.2)	[°C]
Spark Timing Sweep	MBT-3 : MBT+3	[CAD]

Apparent heat release rate (AHRR) on a gross basis was computed based on the method outlined in [25], where heat losses were estimated by the Hohenberg correlation [26] (assuming a constant wall temperature of 500 K) and crevice volume was neglected. The ratio of specific heats was assumed to be that of air and evaluated based on crank angle resolved pressure traces and temperature estimations (via the ideal gas law) yielding values in the range of 1.3-1.4 throughout the cycle. The AHRR is integrated to yield the cumulative apparent heat release. Fractions of the cumulative apparent heat release are used to parameterize combustion phasing; for instance, CA10 refers to 10% of the total heat released. The cylinder pressure traces are also utilized to evaluate gross indicated mean effective pressure (gIMEP) and coefficient of variation (COV) as defined in [25]. Additionally, ringing intensity (RI) is calculated using methods described in [27], to assess the intensity of auto-ignition and quantify combustion noise.

A useful parameter to describe SACI operation is the SI percent (%SI), which is the fraction of deflagration heat released, compared to the total heat released [23]. Based on this definition, conventional SI operation would have %SI = 100% since all of the heat release is by the propagating flame front. Conversely, HCCI mode would classify as %SI = 0% as all the heat release occurs after a kinetics-driven auto-ignition. The calculation of (%SI) is obtained by Eq. (4),

$$\%SI = \frac{\sum_{SOC}^{\theta_{AI}} AHRR(\theta)}{\sum_{SOC}^{EOC} AHRR(\theta)} \quad (4)$$

where θ_{AI} refers to the crank angle of auto-ignition (i.e. auto-ignition timing). SOC indicates the start of combustion and is given by the commanded spark timing; EOC is the end of combustion, given by CA90 (90% of the cumulative apparent heat release).

Results

Experimental results showed similar trends at the two engine speeds tested (900 and 1200 RPM) and suggest that the engine is running in SACI mode. The 900 RPM case is discussed first and in greater detail as similar trends exist between the engine speeds. A more succinct analysis of the data is discussed for the 1200 RPM case, pointing out key distinctions and similarities. The full data for the 1200 RPM cases are available in Appendix A.

Apparent Heat Release Rate Analysis

Figure 3 shows the AHRR of three different spark timings (retarded, MBT, and advanced) for the 80°C–2.5% H_2 case. The spark timings are indicated by colored vertical dashed lines on the left side of Fig. 3. All the experiments showed a brief slowdown in AHRR around 338 CAD, which correlates with the piston sweeping in front of and partially occluding the spark plug from the main chamber. It is hypothesized that the piston motion partially quenches the flame kernel. This AHRR feature is labeled in Fig. 3 and it is important to note that this phenomenon is evident in the AHRR for all conditions tested. Later in the cycle, the AHRRs shown in Fig. 3 each produce an inflection point which indicates that the propagating flame has triggered an auto-ignition in the charge gas, decreasing the burn duration. The inflection point for the average AHRR of each experiment was identified by visually locating the point where the AHRR transitioned to a steeper slope, yielding the auto-ignition timing (θ_{AI}) as described by [23].The corresponding SI percentages for each of the AHRRs in Fig. 3 are labeled in the plot.

The most retarded spark timing (MBT-3) in Fig. 3 has the most delayed auto-ignition, the lowest peak AHRR, and longest burn duration. The slow flame propagation of the mixture appears to induce mild auto-ignition near TDC but AHRR plateaus at around 10 J/CAD, possibly because the expanding chamber volume works against the flame development by cooling, quenching, and/or stretching the reaction zones.

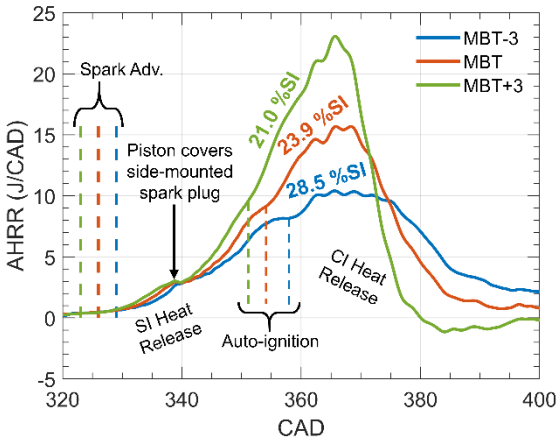

Fig. 3. Sample AHRRs for the 900 RPM, 2.5% H_2, 80°C intake temperature case. The AHRR for MBT spark timing is shown compared to the most retarded and most advanced timings.

The MBT-3 case also exhibits the highest SI percent of the three spark timings shown, indicating that more of its cumulative heat release occurs before auto-ignition. In contrast, the more advanced spark timings (MBT and MBT+3) show advancing auto-ignition timing since the flame begins developing earlier in the compression stroke thereby providing the necessary conditions for auto-ignition earlier in the cycle. Compared to the MBT-3 case, the MBT timing has a more rapid heat release after the auto-ignition point but somewhat plateaus after TDC around 15 J/CAD – similar in trend to the MBT-3 case. Lastly, the most advanced case (MBT+3) auto-ignites earliest and has the highest peak AHRR, lowest SI percent, and shortest burn duration. The greater peak AHRR (~23 J/CAD) contributes to greater heat loss around TDC and more advanced combustion phasing increases the compression work required, both of which contribute to lower gIMEP for spark advancements beyond MBT.

Figure 4 shows a more comprehensive collection of AHRR plots from the experimental study. The left column contains the results from the 40°C intake experiments; the right column shows the cases with an intake temperature of 100°C. The top row of plots shows the 5% H_2 fuel case, the middle row shows 2.5% H_2 and the bottom row shows the 0% H_2 case. Each plot in Fig. 4 corresponds to a specific intake temperature and fueling condition. Within each plot are the AHRRs from the sweep of spark timings, generally from MBT-3 (most retarded) to MBT+3 (most advanced), where the AHRR from the MBT case is shown as a bold purple line in each of the plots. Note that the spark advance for MBT differs for each temperature and fueling condition and is demarcated on each plot with a dashed vertical line.

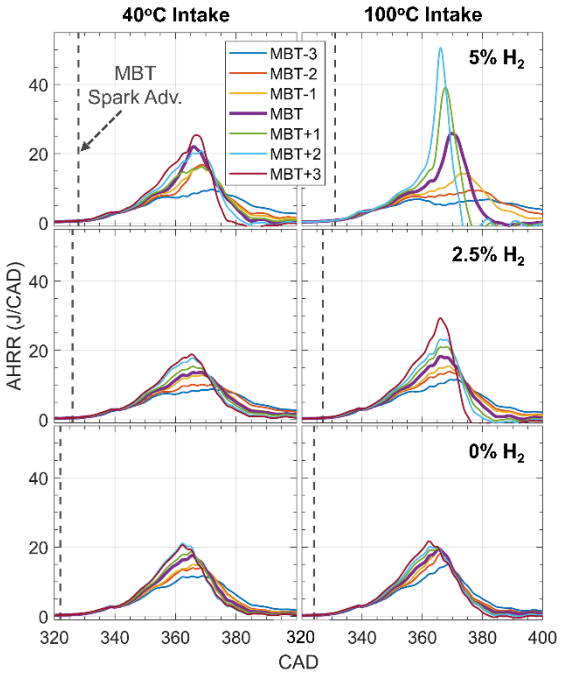

Fig. 4. 900 RPM: AHRR versus CAD for the 40°C (left column) and 100°C (right column) intake temperatures for all fuel compositions (5% to 0% H_2) across spark timings.

The top row of Fig. 4 (5% H_2) illustrates the differences in AHRR for the low and high intake temperature conditions. The 40°C intake case shows similar trends in auto-ignition timing and peak AHRR with advancing spark timing as shown in Fig. 3. However, the 100°C intake case shows that spark timing has a more dramatic impact on AHRR. Auto-ignition triggers a much faster burn and advanced spark timing leads to significantly higher peak AHRR. Indeed, the already high reactivity and flame speed of the mixture is enhanced by the high intake temperature which makes AHRR more sensitive to spark timing. Additionally, the higher flame speed in the 100°C case is compensated for by delaying the spark advance slightly, as can be seen by comparing the dashed vertical lines for spark advance between the left and right plots. The most retarded spark timing (MBT-3) for 100°C–5% H_2 shows somewhat bimodal heat release due to an apparent auto-ignition event around 365 CAD overall resulting in a low AHRR and non-ideal, late combustion phasing. On the other hand, the most advanced spark timing (MBT+2) for 100°C–5%H_2 shows an early and intense auto-ignition event which causes AHRR to peak at around 50 J/CAD, resulting in greater combustion noise (ringing) and heat losses.

Moving to the middle row of plots in Fig. 4, a reduced H_2 concentration in the fuel leads to more consistent AHRR behavior across different spark timings. Advancing spark timing results in shifting the AHRR up and to the left, signifying more rapid

and more advanced heat release. Increasing intake temperature increases the variation, or spread, between AHRRs of different spark timings. The 100ºC–2.5%H_2 case shows that advancing spark timing can result in an AHRR with a sharp peak, but not so much as the 100ºC–5%H_2 case.

Finally, the bottom row shows the results for pure NH_3 fuel at 40ºC and 100ºC intake temperatures. Increasing spark advance has a similar trend to the cases with hydrogen, i.e. increasing peak AHRR and advancing AHRR. An inflection point is evident in each of the AHRRs around 350-360 CAD indicating auto-ignition/SACI mode for each case. Interestingly, increasing the intake temperature to 100ºC for pure ammonia fueling produces negligible impact on the AHRR since peak AHRR and spread with varying spark timing is similar for the two intake temperatures. This result suggests that pure NH_3 engines can be safely operated without knock across a wide range of spark timings and temperature conditions. Adding even as much as 5% H_2 to the fuel poses the possibility of rapid heat release from an auto-ignition event, known as knock, which would need to be cautiously avoided in a potential engine control strategy. Yet, an advantage of hydrogen addition to the fuel is greater impact of spark timing on AHRR which could better provide the needed control when dynamically changing engine load and speed in a production engine [23]. Additionally, as discussed later in this section, hydrogen addition provides a benefit by increasing gIMEP.

AHRR at MBT Timing

Removing the parameter of spark timing, Fig. 5 shows the AHRR for MBT timing for all fuel types at low (40ºC) and high (100ºC) intake temperatures. The top plot of Fig. 5 shows that overall the combustion phasing is very similar for all cases at 900 RPM. Only the AHRR for the 100ºC–5% H_2 case is retarded compared to the other cases. The addition of 5% H_2 enables slightly greater peak AHRR, which facilitates slightly greater gIMEP. The 2.5% H_2 and 0% H_2 cases have similar phasing and peak AHRRs, indicating that despite the fuel differences, a similar AHRR is required for optimal gIMEP.

The bottom plot of Fig. 5 shows that for 1200 RPM, optimal phasing of AHRR is different for the two intake temperatures presented. MBT is achieved with slightly earlier phasing for the 40ºC intake temperature case compared to the 100ºC case, shown by the groupings of blue and red lines in Fig. 5.

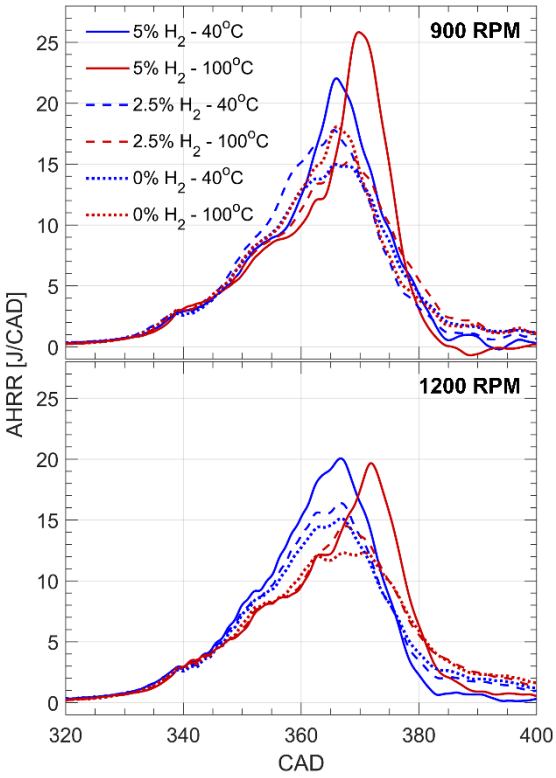

Fig. 5. Apparent heat release rate (AHRR) for MBT timing for all fuels at 900 RPM (top) and 1200 RPM (bottom).

Keeping all else constant, increasing intake temperature would theoretically increase flame speeds for all fueling cases, which was manifested in the experiments by early/rapid auto-ignition, decreased gIMEP, and increased RI. Therefore, the MBT spark timing is retarded at high intake temperature, resulting in later phasing of the 100ºC intake temperature AHRRs shown in Fig. 5. The later phasing of the 100ºC intake temperature case is better captured at the 1200 RPM since less time is available for flame propagation and kinetics to impact phasing on a crank angle basis. Additionally, the 1200 RPM cases show a consistent trend that peak AHRR increases with increasing H_2 concentration for both intake temperatures, in agreement with the fuel reactivity trends.

gIMEP and COV

Engine work output was calculated on an indicated basis using the cylinder pressure traces. Figure 6 shows the gIMEP and COV for the experimental matrix at 900 RPM. The top plot shows the results of the 5% H_2 fuel case for all intake temperature conditions and spark timing. Similarly, the middle and bottom plots show the results from the 2.5% and 0% H_2 fuels, respectively. The left vertical axis shows the gIMEP, the right vertical axis shows the COV, and the spark advance is shown on the horizontal axis.

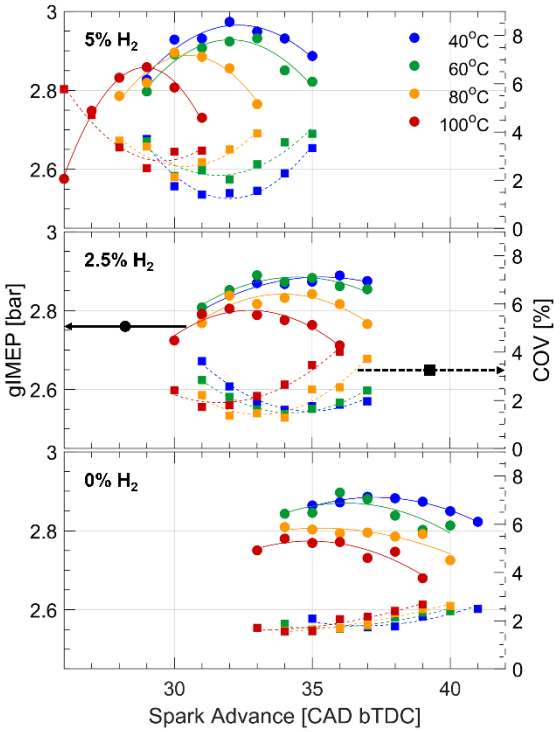

Fig. 6. 900 RPM: Increasing H_2 fraction in the fuel improves gIMEP (left axis) at MBT timing. COV (right axis) behaves inversely to gIMEP.

The top plot shows that for each intake temperature, gIMEP has a unimodal trend with spark advance where optimal gIMEP occurs at MBT timing. As intake temperature increases, the MBT timing is more retarded to account for the increased reactivity and flame speed of the higher-temperature mixture. Additionally, increasing temperature leads to overall decreased gIMEP, which is likely due to differences in combustion phasing, increased heat transfer losses, and less cyclic stability. COV follows an inverse trend compared to the gIMEP, where minimum COV correlates with the maximum gIMEP for each intake condition. Higher intake temperatures result in overall higher COV, indicating greater cycle-to-cycle variation in gIMEP.

The middle plot in Fig. 6 shows the gIMEP and COV of the 2.5% H_2 fuel case where similar unimodal trends exist with spark timing. The optimal spark timing did not vary as much across intake temperatures compared to the 5% H_2 case. The gIMEP and COV curves from different intake temperatures are largely overlapping since they were swept over similar ranges of spark timing. For the low intake temperatures (40-60°C) COV is highest for retarded spark timings and low for advanced spark timings, suggesting that auto-ignition (SACI mode) could be unreliable at retarded timings, causing the engine to switch between SI mode and SACI mode (though auto-ignition is captured by the average AHRR). The opposite is true for the high intake temperatures (80-100°C) which have low COV at retarded spark timings but high COV for advanced timing. Rather than unreliable auto-ignition, the variation for these high temperature cases is likely caused by "knocking cycles" or cycles with rapid heat release compared to the average.

The bottom plot of Fig. 6 shows that for the 0% H_2 (pure ammonia fueling) case, variation in spark timing does not drive large variation in gIMEP. However, there is a slightly parabolic shape to the gIMEP data points, suggesting that some optimal MBT spark timing exists for each temperature. In agreement with other fueling cases, increasing intake temperature decreases gIMEP. By comparison to the other fuel compositions, the 0% H_2 case results in very low COV for all spark timings and temperatures. COV shows a slow rise with increasing spark advance for all temperatures but remains below 3% COV for all the conditions tested.

A comparison of the data point groupings from the top plot down to the bottom plot in Fig. 6 indicates that MBT spark timing advances with decreasing hydrogen fuel fraction. Without H_2 as a combustion promoter, more spark advance is needed to allow time for the flame kernel to develop and propagate. Additionally, a comparison of the plots in Fig. 6 shows that decreasing H_2 fraction leads to slightly decreased gIMEP.

SACI for reduced burn duration

Figure 7 shows the burn duration and RI of all the fueling, intake temperature, and spark timing conditions of the present study. Burn duration, calculated as (CA90-CA10), is shown on the left vertical axis and RI is shown on the right axis, while spark advance is shown on the horizontal. The top, middle and bottom plots of Fig. 7 show the results from the 5% H_2, 2.5% H_2, and 0% H_2 cases, respectively.

Burn duration decreases with increasing spark advance for all fuels and intake temperatures. Increasing the intake temperature shifts the burn duration curve left, as optimal spark timing was more retarded for high intake temperature. Interestingly, all fuels can attain burn durations around 20-35 CAD at the most advanced spark timings. Grannell *et al.* showed that a CFR engine fueled by 100% gasoline exhibited similar burn durations of approximately 30 CAD at a comparable engine speed (1000 RPM) [13]. The laminar flame speeds of these NH_3-H_2 fuel mixtures are 20-25% of that of gasoline (~40 cm/s) [28], yet burn duration can still match that of conventional gasoline operation because of the combustion enhancement from SACI. The chemical heat release is likely

accelerated by auto-ignition of a significant portion of the unburned gases, which increases the total flame surface area beyond that of propagation from a single ignition point as in conventional gasoline SI operation.

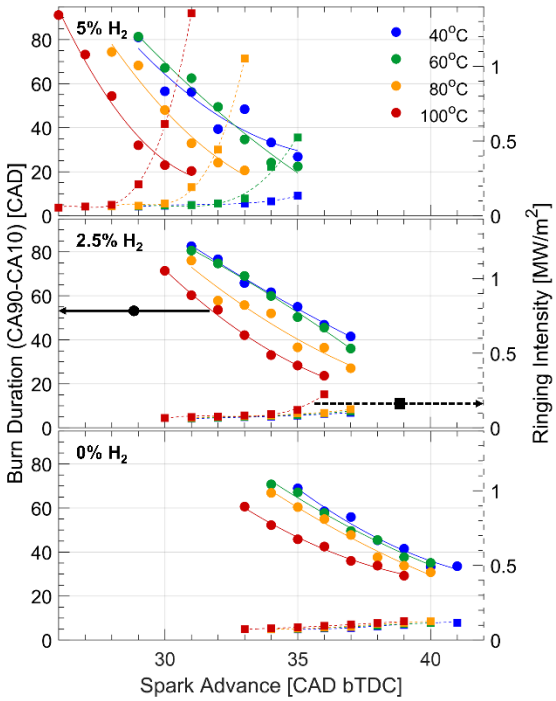

Fig. 7. 900 RPM: Burn duration (left axis) decreases and ringing intensity (right axis) increases with advancing spark timing.

Ringing intensity (RI) presented in Fig. 7 provides further corroborating evidence of SACI operation. Increasing spark advance was shown to augment the intensity of auto-ignition and peak AHRR in a previous section of this work, implying various degrees of SACI. Similarly, RI is a metric for auto-ignition intensity and is shown to increase with increasing spark advance, correlating with decreasing burn duration. The highest level of RI occurs with the 5% H_2 fuel case where RI follows exponentially increasing trends with increasing spark advance. Increasing intake temperature induces ringing at more retarded spark timings. Lower H_2 fuel fractions show a subtler, almost linear, increase in RI with spark advance. Overall, the RIs in the current study are low where the maximum is around 1.5 MW/m^2 – excessive ringing is generally quantified as RI≥5 MW/m^2 (e.g. [29]). Although auto-ignition occurs, NH_3 is resistant to knock, which could be described as more intense auto-ignition with a more instantaneous release of heat and higher RI. While the constraints of RI and combustion noise are typically challenging and require high amounts of EGR for conventional hydrocarbon fuels, the NH_3/H_2 fuel blends tested in the present study are resistant to ringing without sophisticated mixture preparation strategies. However, it is important to note that the current study only considers low-medium engine load (~3 bar gIMEP) so additional experiments are needed to evaluate RI at high load.

SI Percent and Auto-ignition Timing

The SI percent and corresponding auto-ignition timing is shown in Fig. 8. Optimal SI percent in SACI strategies is critical to achieve maximum thermal efficiency within the noise, controllability, and structural constraints for the engine. While the experiments conducted in the present work showed overall low ringing intensity (RI), avoiding knock can be a challenging constraint with conventional hydrocarbon fuels [23].

The 5% H_2 fuel case is shown in the top plot of Fig. 8, with 2.5% and 0% H_2 shown in the middle and bottom plots, respectively. The left vertical axis shows the SI percent, which is the fraction of heat released prior to auto-ignition compared to the total heat released, and the right vertical axis indicates the crank angle where the auto-ignition inflection point occurs in the AHRR for each condition.

Figure 8 shows that SI percent and auto-ignition crank angle decrease with advancing spark timing for all the conditions tested. The top plot of Fig. 8 shows that the 100°C–5% H_2 case is shifted left and curves up to higher SI percentages compared to the other temperatures at this fueling condition. The other intake temperatures seem to have similar slopes for SI percent and auto-ignition timing. The middle and bottom plots of Fig. 8, corresponding to 2.5% H_2 and 0% H_2, respectively, show that SI percent and auto-ignition timing decrease by about the same rate with increasing spark advance regardless of intake temperature. Increasing intake temperature slightly advances the auto-ignition timing, suggesting that the increased temperatures lead to faster flame speeds which trigger auto-ignition sooner.

Interestingly, the decreasing trend of SI percent with increasing spark advance in the present work is opposite that of SACI with hydrocarbon fuels such as gasoline or iso-octane [23,30,31]. SI percent increases with advancing spark timing for SACI with hydrocarbon fuels when holding load and mixture preparation constant. These seemingly incompatible trends are explained by the sensitivity of auto-ignition timing to spark advance.

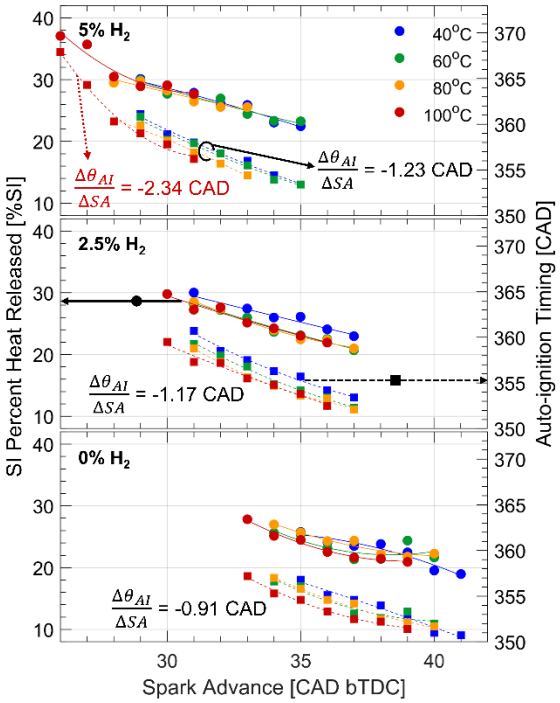

Fig. 8. 900 RPM: SI percent (left axis) and auto-ignition timing (right axis) decrease with advancing spark timing for all fueling and intake temperature conditions.

The average slopes of auto-ignition timing with respect to spark advance ($\frac{\Delta\theta_{AI}}{\Delta SA}$) are noted on each plot in Fig. 8. Notice in the top plot of Fig. 8 that the 100ºC–5% H_2 case was evaluated separately since it was distinct of other temperatures; a single CAD change in spark advance at this condition resulted in ~2.34 CAD change in auto-ignition timing. The other intake temperatures with 5% H_2 fuel resulted in an auto-ignition timing sensitivity of ~1.23 CAD per degree of spark advance. Decreasing the amount of H_2 in the fuel resulted in decreasing sensitivity of auto-ignition timing to spark advance (~1.17 CAD for 2.5% H_2 and ~0.91 CAD for 0% H_2). In their review paper, Robertson et al., inferred a map of auto-ignition timing sensitivity to spark timing across different EGR fractions and equivalence ratios for Mazda's gasoline-fueled SACI engine [23,31]. High amounts of EGR (25-40%) are used to operate within practical design constraints of SACI such as combustion noise, pressure rise rates, engine structural integrity, and other variables. Such operating regimes that satisfy these constraints result in auto-ignition sensitivity to spark timing around 0.2-0.4 CAD, which is considerably less than the auto-ignition sensitivities measured in the current study. Overall, a 1 CAD change in spark timing for the NH_3/H_2-fueled engine of the present study induces significant (0.9-1.2 CAD) change in auto-ignition timing while hydrocarbon-fueled SACI engines result in very small changes (0.2-0.4 CAD) in auto-ignition timing.

Consider a typical AHRR for an SACI cycle, such as the ones shown in Fig. 3. After the onset of spark, the slow deflagration heat release begins, until it is accelerated by an auto-ignition event. If the timing of the auto-ignition event remains nominally the same when advancing spark timing, the duration of deflagration heat release will increase thus increasing SI percent. This increased duration for deflagration heat release occurs in hydrocarbon-fueled SACI since auto-ignition timing is largely unaffected by change in spark timing [23]. The NH_3-fueled engine of the current study shows that advancing spark timing results in a similar advance in auto-ignition timing, thereby keeping the deflagration burn duration about the same. The net effect of shifting the deflagration burn earlier relative to TDC is a decreased SI percent with advancing spark.

This result leads to the question, "why does auto-ignition timing follow spark advance with NH_3 but remain largely unchanged by spark advance for hydrocarbon fuels?" Robertson et al. suggest that as spark is retarded, more auto-ignition energy is supplied by compression from the piston rather than from the deflagration flame front. Given that auto-ignition timing responds strongly to spark timing in the present study, it is hypothesized that the majority of ignition energy must be supplied by the deflagration flame front. This may be due to the high ignition energy of NH_3 which is four orders of magnitude that of gasoline [32], or that the auto-ignition temperature of ammonia is nearly double that of gasoline [19]. Such resistance to auto-ignition could mean that a deflagration flame is critical to create conditions suitable for auto-ignition.

Comparison to 1200 RPM

The same range of fuel, intake temperature, and spark timing experiments were conducted at an increased engine speed of 1200 RPM. Figure 9 presents the parameters shown in Figs. 6-8 for a single fuel condition (2.5% H_2) at 1200 RPM to concisely show the impact of increasing engine speed. The top plot shows the gIMEP and COV, the middle plot shows the burn duration and RI, and the bottom plot shows the SI Percent and auto-ignition timing. Each of these plots are comparable to the 2.5% H_2 fuel condition in Figs. 6-8.

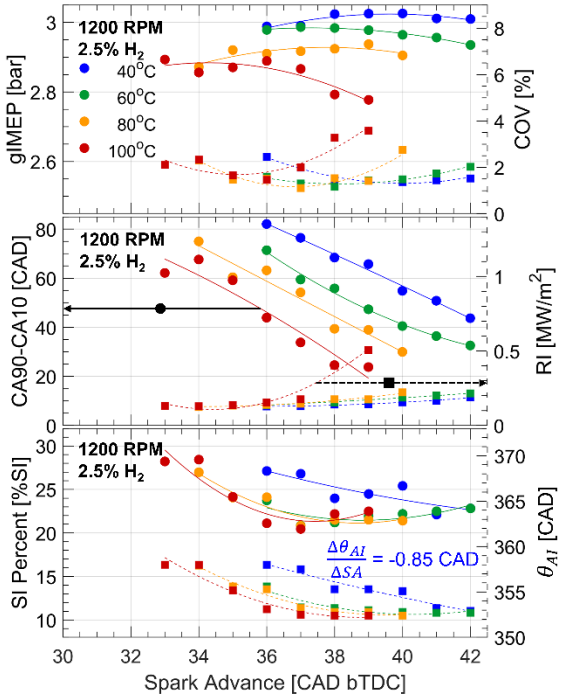

Fig. 9. 1200 RPM results for 2.5% H_2 fuel case showing gIMEP and COV (top), burn duration and RI (middle), and SI percent and auto-ignition timing (bottom).

The top plot of Fig. 9, shows that there is slight variation in gIMEP with spark timing, and that increased intake temperature decreases gIMEP, in agreement with the 900 RPM case. COV behaves somewhat inversely to gIMEP where the lowest COV tends to produce the greatest gIMEP. It should be pointed out that the in-cylinder charge mass per cycle was equivalent between the two engine speeds, but the gIMEP for the 1200 RPM case was greater than the corresponding 900 RPM cases. The 1200 RPM case showed slightly improved combustion efficiency, possibly due to enhanced turbulence and reduced heat loss, which contributes to improve gIMEP.

The middle plot of Fig. 9 shows that burn duration decreases and RI increases with increasing spark advance, in agreement with the 900 RPM cases. However, the 100°C intake temperature case shows a more appreciable increase in RI than the 900 RPM case at advanced spark timing.

Unlike the top two plots in Fig. 9, SI percent and auto-ignition timing in the bottom plot follow a different trend than they did for the 900 RPM case. Recall that Fig. 8 shows that advancing spark timing decreased SI percent and advanced the auto-ignition timing. This trend is consistent with the 40°C case at 1200 RPM, which shows autoignition timing sensitivity of ~0.85 CAD per degree of spark advance. However, other intake temperatures in Fig.9 show that advancing spark timing could result in an increasing SI percent and a steady auto-ignition timing. For example, the 100°C case plainly shows that advancing spark initially decreases SI percent, but then increases it. Meanwhile, the auto-ignition timing initially decreases with advancing spark timing, but it eventually converges to a steady value.

The correlation between auto-ignition timing and SI percent supports the argument that SI percent is closely linked with the sensitivity of auto-ignition timing to spark timing. These results suggest that the SI percent trend is rooted in whether the energy for auto-ignition is primarily supplied by the propagating flame front or by the compression due to the piston movement. At 1200 RPM a faster moving piston with a preheated intake charge delivers a more dominant amount of ignition energy to the unburned mixture than the propagating flame front. An additional consideration is that increasing engine speed typically enhances in-cylinder turbulence which could strongly impact SACI behavior. The CFR engine is known to have an overall quiescent combustion chamber, thus the results shown here are not subject to the swirl/tumble charge motion typical of production engines. Previous work has shown that enhanced swirl in SACI engines increases the turbulent flame speed, and delays auto-ignition timing [33] and SACI mode has been achieved in an NH_3-fueled ICE with a swirl number of 2.3 [8]. Comprehensive understanding of the impact of charge motion and turbulence on SACI mode in an NH_3-fueled engine is beyond the scope of this experimental work, but certainly an important topic for future work.

Emissions

Selected cases show the broad impact of changing fuel hydrogen fraction, intake temperature, and engine speed on emissions in Fig. 10. Low temperature cases (40°C) are shown in shades of blue, where the royal blue indicates 5% H_2 fuel, and dark blue indicates 0% H_2. Similarly, high temperature (100°C) cases are shown by the red bars in Fig. 10, light red indicates the cases with 5% H_2 and dark red represent 0% H_2. The shaded portions of Fig. 10 encompass data which was acquired at 1200 RPM engine speed, unshaded portions represent the 900 RPM cases.

Due to the uncertainty in dilution ratio error bars are significant for NH_3, NO, and N_2O (NO_2 was also measured, but concentrations in the diluted sample were within the signal noise for the detector). O_2 was measured directly, without dilution, so it was measured with greater confidence. Given that many of the error bars overlap one another, trends in emissions must be interpreted cautiously. Based on Fig. 10, adding H_2 to the fuel generally reduces NH_3 emissions. Increasing intake temperature also

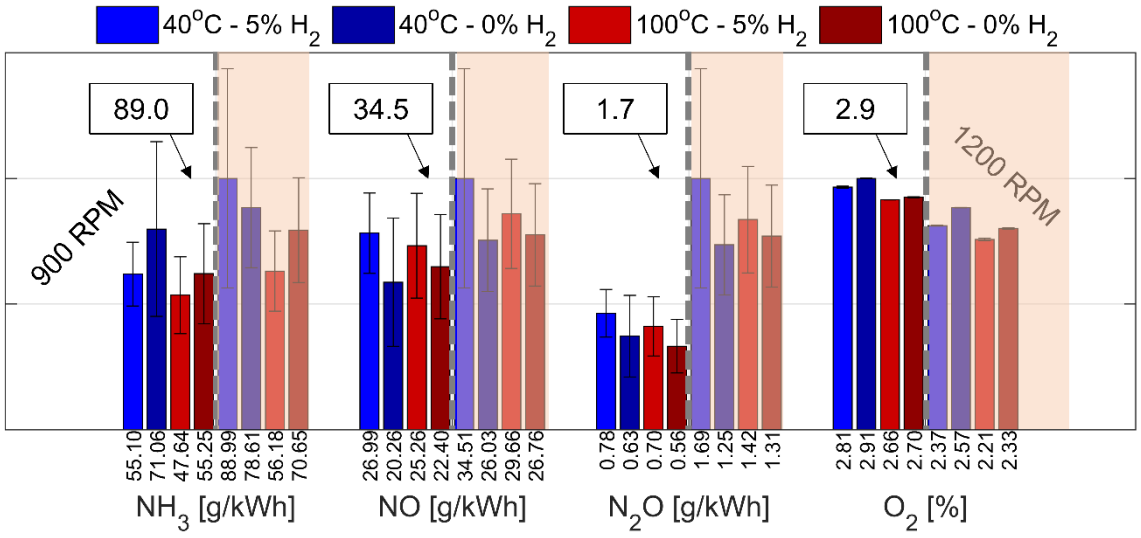

Fig. 10. Emissions results at select fuel and temperature cases where the shaded and unshaded regions correspond to 1200 RPM and 900 RPM, respectively.

mitigates unburned NH_3 emissions on an indicated specific basis, despite the reduced gIMEP at these high temperature conditions (refer to Figs. 6 and 9). These results agree with intuition that enhanced reactivity and flame speed, either through a combustion promoter or preheating, leads to more complete consumption of NH_3.

On the other hand, increasing H_2 fuel fraction produces more NO but changing intake temperature does not show a clear trend. Indeed, the 5% H_2 cases likely have higher peak combustion temperatures favoring the formation of thermal NO_x via the Zel'dovich mechanism, and less NH_3 is available for non-catalytic reduction of NO, compared to the 0% H_2 cases. Increasing engine speed from 900 RPM to 1200 RPM increased NO emissions slightly. These measurements must also reckon with large error bars so conclusive quantitative interpretation of these results is not possible.

N_2O is a remnant of incomplete ammonia combustion [28] and is definitively higher for the 1200 RPM cases compared to 900 RPM, even considering the uncertainty of measurements. The reduced time for combustion at the greater engine speed is the likely reason for less complete reactions and thus greater N_2O emissions. Furthermore, despite the error bar overlap, the nominal N_2O measurements appear to decrease with decreasing H_2 fuel fraction and increasing temperatures.

Engine-out O_2 emissions range around 2-3% for all test conditions even though the mixture is stoichiometric. These combustion inefficiencies are likely related to the slow flame speed of ammonia and trapping of the fuel/air mixture in the engine crevices. The high compression ratio (18:1) of the present experiments forces a greater mass fraction of the charge gas into the crevices than would be typical of a conventional SI engine compression ratio (~10:1). As expected, increasing the reactivity of the mixture, either through hydrogen addition or increasing intake temperature decreases O_2 emissions, improving combustion efficiency. Additionally, increasing engine speed reduces O_2 emissions, possibly because more oxygen combines with nitrogen to form higher levels of NO and N_2O for the high-speed case. A slight increase in turbulence is expected at increased engine speed, which may enhance flame speed thereby accounting for some of the decrease in O_2 emissions.

Conclusions

A CFR engine fueled by NH_3 and NH_3/H_2 blends was operated across a wide range of intake temperatures and spark timings for two different engine speeds. High compression ratio enables SACI mode for this range of operating conditions as evidenced by the average AHRRs, combustion durations, and ringing intensities. The SACI behavior was quantified by the auto-ignition timing and SI percent of heat release. Key emissions were measured for these engine operating conditions including unburned NH_3, NO, N_2O, and O_2. From these experiments conducted at low/medium engine load, the following conclusions are drawn.

- AHRRs are sensitive to H_2 fuel fraction, intake temperature, and spark timing though all cases exhibit an inflection point where AHRR increases more quickly and is considered the auto-ignition timing.
- Increasing H_2 fuel fraction benefits gIMEP, but deviating from MBT timing leads to greater instability. Pure NH_3 operation is most robust to

varying spark timing without danger of knock or inhibiting performance significantly.

- Combustion duration is similar to that of a gasoline-fueled CFR engine operating in conventional SI mode. SACI enhances the burn rate to overcome the flame speed limitation of NH_3 blended with small H_2 fractions (20-25% the laminar flame speed of gasoline).
- Ringing intensity increases with advancing spark timing (and advancing auto-ignition timing), but is always well below the safe operating limit of 5 MW/m^2.
- SI percent decreases with increasing spark advance at 900 RPM, which is opposite the trend noted in hydrocarbon-fueled SACI engines. The high sensitivity of auto-ignition timing to spark advance implies that ignition energy is primarily supplied by the deflagration flame front, rather than the compression from the piston.
- NH_3 emissions are hypothesized to be primarily driven by the charge mass trapped in the crevices, however they seem to be mitigated by increased H_2 fraction and increased intake temperature. Conversely, increasing H_2 fraction and intake temperature leads to increased NO emissions. N_2O is definitively higher for the higher engine speed, since there is less time for this intermediate species to fully react.

Overall, the high knock-resistance of ammonia enables SACI, which could be a solution to its low flame speed without blending large amounts of hydrogen. Operating with a high compression ratio could also improve thermal efficiency. Given that the CFR engine was the platform for these experiments, cylinder charge motion was not considered in the experimental study. Additional investigation of engine speed, load, and cylinder charge motion/turbulence, which likely have strong influence on the auto-ignition phenomenon of SACI, would be topics of future work.

Acknowledgments

This research was funded through an appropriation from the State of Minnesota Renewable Development Account to the University of Minnesota West Central Research and Outreach Center.

Conflicts of Interest

The authors declare no conflict of interest. The funders had no role in the design of the study; in the collection, analyses, or interpretation of data; in the writing of the manuscript, or in the decision to publish the results.

Appendix A

Figures A1-A3 show the results of 1200 RPM engine speed for comparison with the 900 RPM results shown in Figs. 6-8 in the main body of this work. Overall, Figs. A1-A2 show similar trends to the 900 RPM cases (Figs. 6-7). However, Fig. A3 shows that SI percent and auto-ignition timing respond differently to spark timing compared to the 900 RPM cases. These distinct trends in the 1200 RPM data are discussed in the results section of this work, using the 2.5% H_2 fuel case as a representation of the faster engine speed.

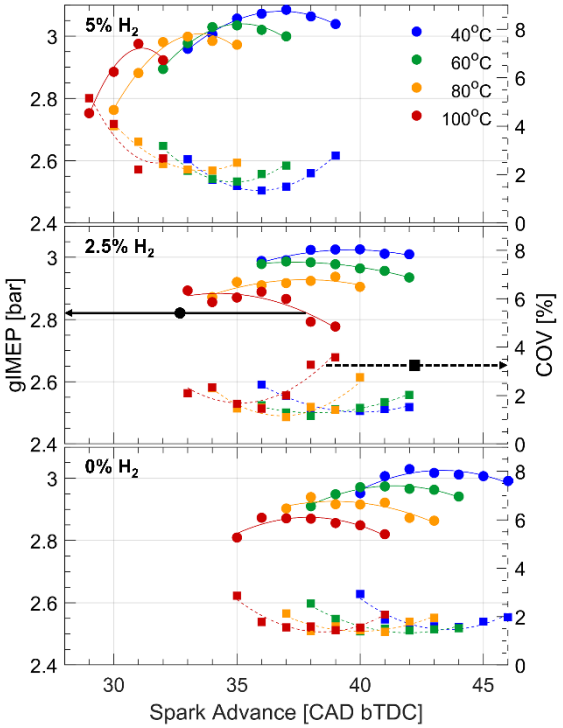

Fig. A1. gIMEP was improved by increasing engine speed to 1200 RPM. Increasing H_2 fraction in the fuel improves gIMEP at MBT timing and increases sensitivity of gIMEP and COV to spark timing.

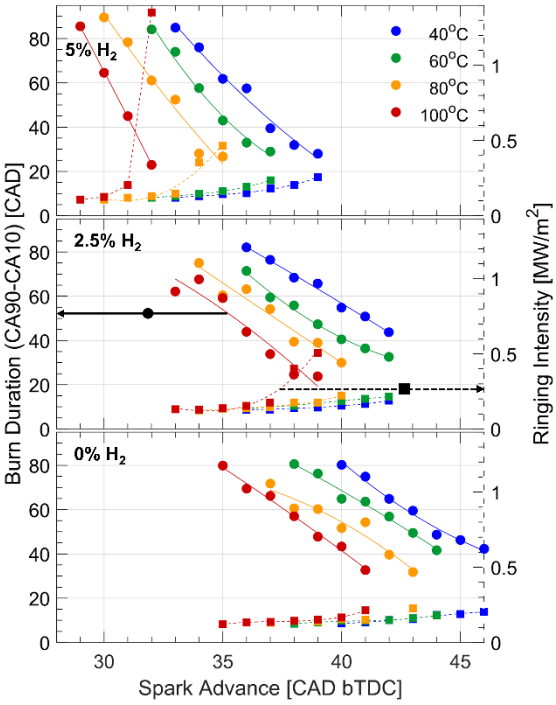

Fig. A2. Burn duration decreases and ringing intensity (RI) increases with advancing spark timing; trends are consistent between engine speeds.

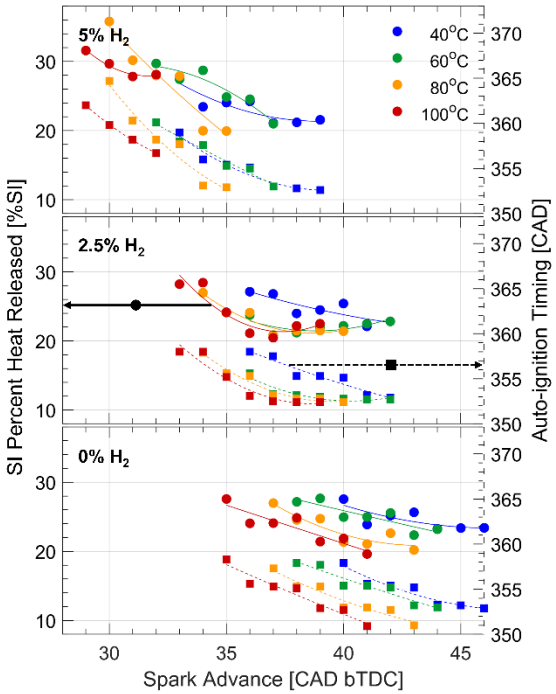

Fig. A3. SI percent and auto-ignition timing are not always monotonic at 1200 RPM. SI percent decreases when auto-ignition timing is sensitive to spark timing; steady auto-ignition timing with varying spark advance correlates with increasing SI percent.

References

1. Williams JH, Jones RA, Haley B, Kwok G, Hargreaves J, Farbes J, et al. Carbon-Neutral Pathways for the United States. AGU Adv. 2021; 2(1): 1-25; doi: https://doi.org/10.1029/2020AV000284

2. European Commission. A Clean Planet for All: A European Strategic Long-Term Vision for a Prosperous, Modern, Competitive, and Climate Neutral Economy. Communication from the Commission. 2018; 1-25.

3. Stern N, Xie C. China's New Growth Story: Linking the 14th Five-Year Plan with the 2060 Carbon Neutrality Pledge. JCEBS. 2022; 1-21; doi: https://doi.org/10.1080/14765284.2022.2073172

4. Valera-Medina A, Amer-Hatem F, Azad AK, Dedoussi IC, de Joannon M, Fernandes RX, et al. Review on Ammonia as a Potential Fuel: From Synthesis to Economics. Energy Fuels. 2021; 35: 6964-7029; doi: https://doi.org/10.1021/acs.energyfuels.0c03685

5. Chehade G, Dincer I. Progress in Green Ammonia Production as Potential Carbon-Free Fuel. Fuel. 2021; 299: 120845; doi: https://doi.org/10.1016/j.fuel.2021.120845

6. Hydrogen and Fuel Cell Technologies Office. Hydrogen Storage. Multi-Year Research Development and Demonstration Plan. DOE, EERE; 2015.

7. Muralidharan N, Self EC, Dixit M, Du Z, Essehli R, Amin R, et al. Next-Generation Cobalt-Free Cathodes - A Prospective Solution to the Battery Industry's Cobalt Problem. Adv. Energy Mater. 2022; 33-53; doi: http:// dx.doi.org/ 10.1002/aenm.202103050

8. Mounaïm-Rousselle C, Mercier A, Bréquigny P, Dumand C, Bouriot J, Houillé S. Performance of Ammonia Fuel in a Spark Assisted Compression Ignition Engine. Int J Engine Res. 2021 August; 23(5); doi: https://doi.org/10.1177/14680874211038726

9. Reggeti SA, Kane SP, Northrop WF. Hydrogen Production in Ammonia-Fuelled Spark Ignition Engines. Appl Energy Combust Sci. 2023 June; 14(100136); doi: https://doi.org/10.1016/j.jaecs.2023.100136

10. Kroch E. Ammonia - A Fuel for Motor Buses. J Inst Petroleum. 1945; 31: 213-223.

11. Pearsall TJ, Garabedian CG. Combustion of Anhydrous Ammonia in Diesel Engines. SAE Transactions. 1968; 76(4): 3213-3221. https://doi.org/10.4271/670947

12. Cornelius W, Huellmantel LW, Mitchell HR. Ammonia as an Engine Fuel. SAE Transactions. 1966; 74: 300-326. https://doi.org/10.4271/650052

13. Grannell SJ, Assanis DN, Bohac SV, Gillespie DE. The Fuel Mix Limits and Efficiency of a Stoichiometric, Ammonia, and Gasoline Dual

Fueled Spark Ignition Engine. J Engin Gas Turbines Power. 2008 July; 130(4); https://doi.org/10.1115/1.2898837
14. Ryu K, Zacharakis-Jutz GE, Kong SC. Effects of Gaseous Ammonia Direct Injection on Performance Characteristics of a Spark Ignition Engine. Appl Energy. 2014 March; 116(1): 206-215; doi: https://doi.org/10.1016/j.apenergy.2013.11.067
15. Gill SS, Chatha GS, Tsolakis A, Golunski SE, York APE. Assessing the Effects of Partially Decarbonising a Diesel Engine by co-fuelling with dissociated ammonia. Int J Hydrogen Energy. 2012 April; 37(7): 6074-6083; doi: https://doi.org/10.1016/j.ijhydene.2011.12.137
16. Kane SP, Northrop WF. Thermochemical Recuperation to Enable Efficient Ammonia-Diesel Dual-Fuel Combustion in a Compression Ignition Engine. Energies. 2021 November; 14(22); doi: https://doi.org/10.3390/en14227540
17. Lhuillier C, Brequigny P, Contino F, Mounaim-Rousselle C. Experimental Study on Ammonia/Hydrogen/Air Combustion in Spark Ignition Engine Conditions. Fuel. 2020 June; 269; doi: https://doi.org/10.1016/j.fuel.2020.117448
18. Frigo S, Gentili R. Analysis of the Behaviour of a 4-Stroke SI Engine Fuelled with Ammonia and Hydrogen. Int J Hydrogen Energy. 2013 February; 38(3): 1607-1615; doi: https://doi.org/10.1016/j.ijhydene.2012.10.114
19. Mounaïm Rousselle C, Bréquigny P, Dumand C, Houillé S. Operating Limits for Ammonia Fuel Spark-Ignition Engine. Energies. 2021 July; 14(14); doi: https://doi.org/10.3390/en14144141
20. Comotti M, Frigo S. Hydrogen Generation System for Ammonia-Hydrogen Fuelled Internal Combustion Engines. Int J Hydrogen Energy. 2015; 40(33): 10673-10686; doi: https://doi.org/10.1016/j.ijhydene.2015.06.080
21. Wang W, Herreros JM, Tsolakis A, York APE. Ammonia as Hydrogen Carrier for Transporation; Investigation of the Ammonia Exhaust Gas Fuel Reforming. Int J Hydrogen Energy. 2013 August; 38(23): 9907-9917; doi: https://doi.org/10.1016/j.ijhydene.2013.05.144
22. Alger T, Mangold B. Dedicated EGR: A New Concept in High Efficiency Engines. SAE Int J Engines. 2009; 2(1): 620-631; doi: https://doi.org/10.4271/2009-01-0694
23. Robertson D, Prucka R. A Review of Spark-Assisted Compression Ignition (SACI) Research in the Context of Realizing Production Control Strategies. SAE Technical Paper. 2019; 24(0027); doi: https://doi.org/10.4271/2019-24-0027
24. Chiodi M, Kaechele A, Bargende M, Wichelhaus D, Poetsch C. Development of an innovative Combustion Process: Spark-Assisted Compression Ignition. SAE Int J Engines. 2017; 10(5): 2486-2499; doi: https://doi.org/10.4271/2017-24-0147
25. Heywood JB. Internal Combustion Engine Fundamentals: McGraw-Hill Education; 2018.
26. Hohenberg GF. Advanced Approaches for Heat Transfer Calculations. SAE Transactions. 1979; 88(3): 2788-2806. https://doi.org/10.4271/790825
27. Eng J. Characterization of Pressure Waves in HCCI Combustion. SAE Technical Paper. 2002; 01(2859); doi: https://doi.org/10.4271/2002-01-2859
28. Kobayashi H, Hayakawa A, Somarathne KDK, Okafor EC. Science and Technology of Ammonia Combustion. Proc Combust Inst. 2019 November; 37(1): 109-133; doi: https://doi.org/10.1016/j.proci.2018.09.029
29. Dernotte J, Dec J, Ji C. Investigation of the Sources of Combustion Noise in HCCI Engines. SAE Int J Engines. 2014 July; 7(2): 730-761; doi: https://doi.org/10.4271/2014-01-1272
30. Olesky LM, Martz JB, Lavoie GA, Vavra J, Assanis DN, Babajimopoulos A. The Effects of Spark Timing, Unburned Gas Temperature, and Negative Valve Overlap on the Rates of Stoichiometric Spark-Assisted Compression Ignition Combustion. Appl Energy. 2013 May; 105: 407-417; doi: https://doi.org/10.1016/j.apenergy.2013.01.038
31. Matsumoto K, Urushihara T, Inoue A, Kawai Y, Miyamoto T, Koshiro Y, inventors; Engine Control Device. European Patent patent EP 3421766. 2017 August 24.
32. Fernandez-Tarrazo E, Gomez-Miguel R, Sanchez-Sanz M. Minimum Ignition Energy of Hydrogen-Ammonia Blends in Air. Fuel. 2023 April; 337: 127128; doi: https://doi.org/10.1016/j.fuel.2022.127128
33. Persson H, Johansson B, Remon A. The Effect of Swirl on Spark Assisted Compression Ignition (SACI). SAE Transactions. 2007; 116(4): 334-344; doi: https://doi.org/10.4271/2007-01-1856